Molecular charge transport : relating orbital structures to the conductance properties

Guédon, C.M.

5

Conductance properties of a series of OPE molecules

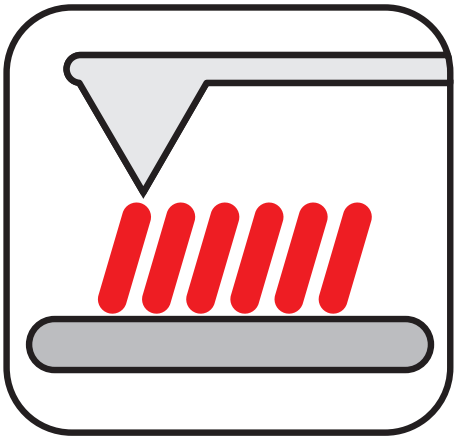

In this chapter we present charge transport measurements on a series of organic molecules with different lengths composed of identical building blocks. The synthesized oligo-phenyl-ethynylene (OPE) molecules are investigated both in their dithiolated and monothiolated form. We perform our experiments using a conducting probe atomic force microscope (C-AFM). Those measurements enable us to scrutinize two important concepts in molecular electronics. (i) The length dependence of molecular conductance. (ii)Transition voltage spectroscopy (TVS).

5.1 Introduction

The relation between chemical structure and charge transport properties is at the heart of molecular electronics. Hence, to understand the physics behind it, experiments have been conducted that vary the chemical structure of the molecules as well as the methodology to extract information from the obtained data. From the start, the length dependence of conductance has enjoyed large attention in field of molecular electronics[1, 2]. Indeed, quickly, the analogy with a tunnel junction was made, as the conductance was found to be exponentially dependent on length, resulting in the expression of this length dependence in the so called β-factor, the exponential decay constant. Furthermore this length dependence has been measured in a wide variety of devices resulting in a wide range of β-values[2]. Therefore it has become a popular benchmark to validate new measuring methods[3, 4]. Still the β-factor is an ill defined concept in molecular junctions as we will point out later on.

5.2 Experimental details

The chemical structure of the molecules, synthesized by Hennie Valkenier at Groningen university [5], used in this work are presented in figure 5.1. Self-Assembled Monolayers (SAMs) of the acetyl-protected mono- and dithiols were grown from solutions with triethylamine as deprotecting agent, which promotes the formation of high-quality and densely-packed SAMs[6]. These SAMs were grown from 0.5 mM solutions in THF (anhydrous) with 10% (v/v) triethylamine (Fisher, HPLC grade, degassed) added. All solutions and SAMs were prepared inside a glovebox filled with nitrogen (<5 ppm O_2)[1]. We used freshly prepared samples of 150 nm gold on mica for the ellipsometry and XPS studies, and freshly prepared samples of 5 nm chromium and 200 nm gold thermally deposited on a silicon wafer for the CP-AFM studies. Samples were immersed upside down for two nights in about 3 mL solution. After this immersion time,

[1]The SAM's are prepared by Hennie Valkenier at the University of Groningen

the samples were taken from solution, rinsed three times with clean THF, and dried under the nitrogen atmosphere in the glovebox. Conducting atomic force

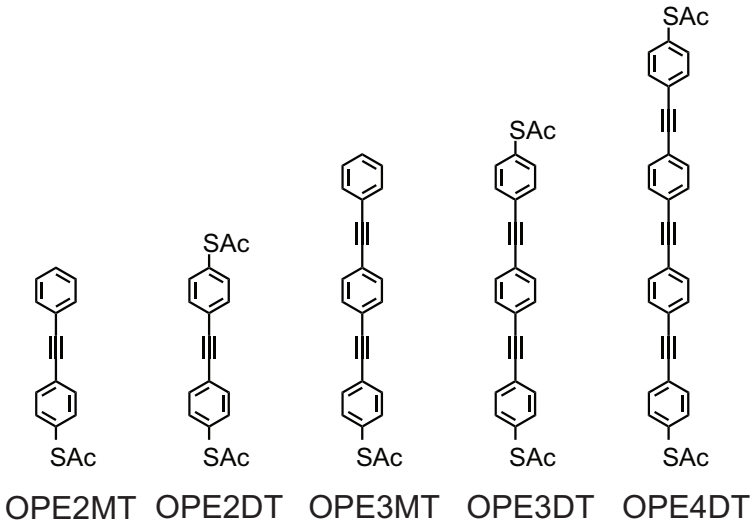

FIGURE 5.1: **Chemical structure of the molecules measured.** The oligo (phenylene ethynylene) (**OPE**) series here shown in which the length of the OPE molecules increases with one phenylene ethynylene unit per molecule (**2**,**3** and **4** rings). In addition to that each OPE is found in a dithiloated form (**DT**) and a monothiolated from (**MT**) both acetyl protected.

microscopy (C-AFM) is performed on a commercial AFM (Digital Instrument). A Multimode AFM base is used in combination with a Nanoscope IIIa controller and Nanoscope V6r13 software. The conductance measurements are performed in contact mode i.e. the feed-back is done on the deflection set point in order to apply a force of typically 2 nN on the SAM. During the conductance measurements the scanning is disabled. The AFM cantilevers used are NP-10 (Veeco) of type B ($f_0 = 14 - 26$ kHz and $k = 0.12N/m$). The SiN AFM tips are coated by sputtering with MoGe (4nm) as an attachment layer and subsequently with 80 nm of Au. A scanning electron micrograph of a typical cantilever is shown in figure 5.2 The electrical measurements are controlled by a labview program and interfaced by a 16 bit NI data acquisition card. The substrate carrying the SAM is biased while the tip is grounded. While the bias voltage is swept (typically from 0 V to -1 V to 1 V and back to 0 V) the current is recorded at a sampling rate of 10 kHz and 1000 points are taken per curve. To do so the current is amplified using a Femto DLPCA-200 variable gain current amplifier. For each

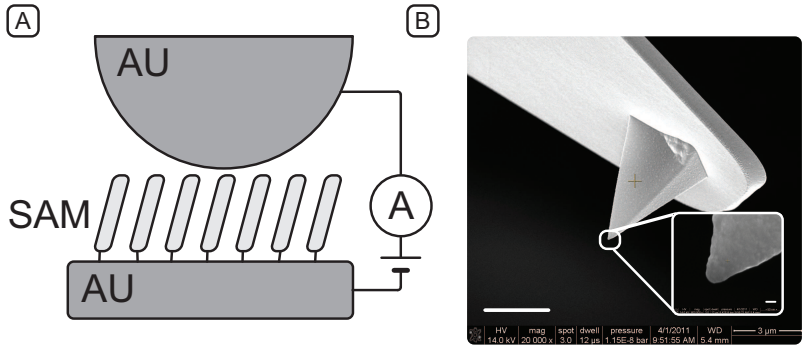

FIGURE 5.2: **SEM picture of a C-AFM cantilever.** SEM picture of a AFM cantilever coated with 4nm MoGe and 80 nm Au. The scale bar is 3μm and 50 nm for the inset.

measurement spot 100 to 1000 I(V)-curves are recorded, for each sample 2 to 8 spots are probed.

Subsequently the I(V) curves are smoothed with a local regression using weighted linear least squares and a 2nd degree polynomial model. Next we take a numerical derivative of the current relative to the voltage (dI/dV). Finally we construct a 2D histogram of these dI/dV values by logarithmically binning them for each bias voltage and plotting them next to each other. This will result in a 3D graph with on the x-axis the bias voltage, on the y-axis the log (dI/dV) and on the z-axis (in colour scale) the number of counts. Such a 2D histogram can be seen as a collection of traditional 1D conductance histograms for different bias voltages. In figure 5.3 we show such a 2D histogram with the related cross-section 1D histograms, taken at various bias voltages, to illustrate this method of plotting our data.

This representation enables us to distinguish general tendencies in dI/dV-curves from statistical variations in the conductance values themselves. In addition to that such plots represent the whole dataset ($\approx$ 2000 traces) at once without the need of data selection or further processing. Indeed this is a recurrent problem in molecular electronics, how to deal with the large variation conductance values? Selecting data [7–9], leads to a biased view of the results depending on the criteria used. Indeed the selection is not always based on

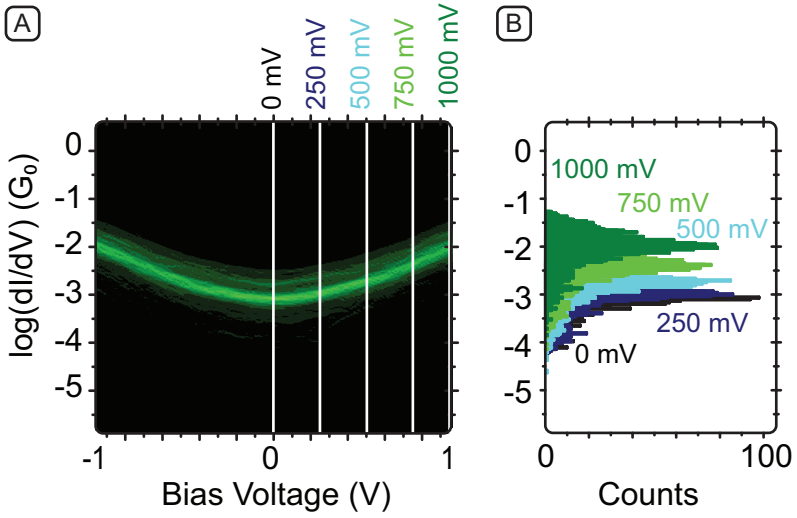

FIGURE 5.3: **2D histogram and its corresponding 1D histograms. A** 2D histogram for the OPE4DT molecule, the vertical lines denote the corresponding 1D histograms shown in **B** for 0, 250, 500, 750 and 1000 mV.

statistical principles which can alter the understanding of the experimental results [10]. Averaging data is a processing tool that is widely used [11–13] and presents the risk of over or under -expressing some values depending on the type of averaging e.g. linear or logarithmic averaging. In addition, averaging smears out information present in the data and removes the relevant intrinsic variations present in the data. Representing our data in the form of 2D histograms avoids the problems mentioned above. The data for OPE2MT were not reproducible as the conductance values varied too much and the tip crashed into the substrate regularly probably due to large defects in the SAMs.

5.3 CHARGE TRANSPORT MEASUREMENTS

In figure 5.4 A-C we show the 2D histograms for the dI/dV of OPE2DT, OPE3DT and OPE4DT. First let us discuss their similar shape. Indeed, the graphs show a symmetric valley-like shape for the whole range of bias voltage. Here we can clearly see the advantage of these histograms, the shape is easily distinguishable, independently of the conductance variations intrinsic to molecular charge transport. The observed symmetric parabola-like shape is expected for symmetric molecular junctions. As we have seen in chapter 1 we can relate

the transmission function T(E) of a junction to the current flowing through it when biased with a voltage eV using the Landauer formalism (equation 5.1).

$$I = \frac{2e}{h}\int_{-\infty}^{\infty} T(E,V)(f_R(E) - f_L(E))dE \tag{5.1}$$

With $f_{R,L}$ being the Fermi-Dirac function for the right and left electrodes with electrochemical potential $E_f - (1-\eta)eV$ and $E_f - \eta eV$ respectively and η being the parameter describing the symmetry of the voltage drop over the junction. For $T = 0$ K we can derive the expression for the first derivative of the current, dI/dV (equation 5.2).

$$\frac{dI}{dV} = \eta T(\eta eV) + (1-\eta)T((1-\eta)eV) \tag{5.2}$$

As an important consequence, symmetric dI/dV-curves are necessarily obtained for symmetrically coupled molecules, irrespective of the (a)symmetry of T(E) around the Fermi level E_F. This is easily seen by inserting $\eta = 0.5$ into the formula above, and interchanging $+V$ and $-V$. Consequently for any transmission function, $T(E)$, the resulting dI/dV curve is symmetric around zero bias and is an average of the $T(E)$ for positive and negative bias voltages. The transmission function for OPE's is, as can be seen in figure 5.5, a valley between the two peaks corresponding to the HOMO and the LUMO. Although it is not symmetric around the Fermi level, the resulting dI/dV does become symmetric for symmetric junctions by virtue of equation 5.2, similar to the measured curves in figure 5.4. In the case of monothiols, like OPE3MT, the junction is asymmetric resulting in an asymmetric voltage drop over the junction and thus in a parameter $\eta \neq 0.5$. It is clear from equation 5.2 that the resulting dI/dV will be asymmetric. Indeed in figure 5.4-D we observe an asymmetric dI/dV for OPE3MT.

5.3.1 Length dependence of the conductance

Let us now concentrate on the trends in the measured conductances for OPE2DT, OPE3DT and OPE4DT. In figure 5.3 we have shown how the 2D histograms are constructed. Of course we can also make a cross-section at each bias to extract a 1D conductance histogram. We therefore can extract the most probable conductance value for each molecule at each bias. The obtained 1D histogram also displays the associated variation in conductance as it is better suited than error bars to visualize the spread in measured values. In figure 5.7-A, the zero bias conductance values (black dots) are plotted as a function of molecular length on a semi-log scale[2]. Hence we notice a roughly exponential dependence of

[2]To determined the lengths the Hyperchem™software release 7.52 is used, the distance from S- to S-atom is calculated.

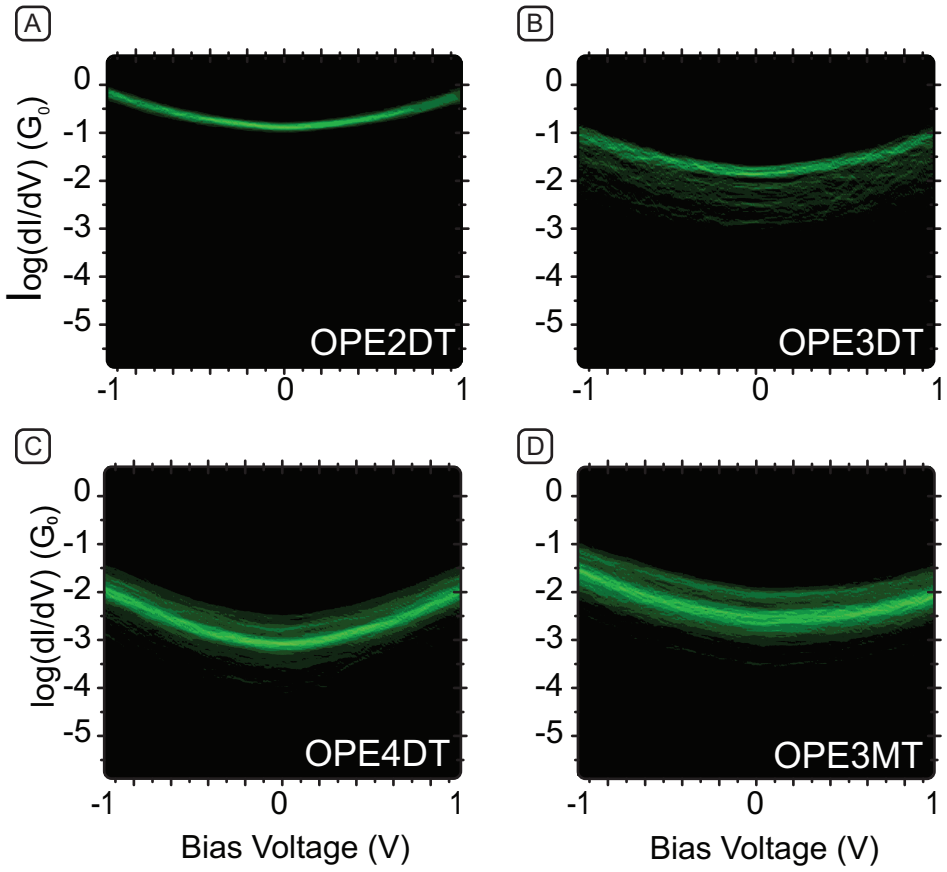

FIGURE 5.4: **Two-dimentional conductance histograms.A-D** show logarithmically binned 2D-histograms of dI/dV (in units of quantum conductance $G_0 = 2e^2/h$) vs. bias voltage V for OPE2DT (**A**), OPE3DT (**B**), OPE4DT (**C**) and OPE3MT (**D**). The colour scale indicates the number of counts and ranges from black (0 counts) to light green (more than 40 counts). The corresponding molecular structures can be found in figure 5.1.

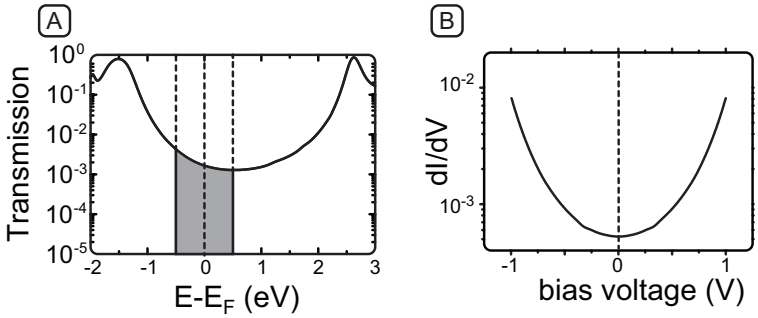

FIGURE 5.5: **Calculated transmission function for OPE3DT. A** Energy dependent transmission function for OPE3DT calculated by Troels Markussen (personal communication) using DFT-NEGF formalism. In gray we indicate the portion of the transmission curve integrated to calculate the current in the junction. **B** We calculate the resulting dI/dV for a symmetric junction with an applied potential V.

the conductance on the molecular length i.e. the conductance is increasing for decreasing lengths. Naively one can make here an analogy with a tunnel barrier and so determine the exponential decay factor β. We will discuss the validity of this analogy later on. Nonetheless, comparing our decay factor of $\beta_{OPE} = 0.35 \pm 0.01$ Å^{-1} with values obtained in the literature (for zero bias conductances) could confirm the validity of our measurement technique. The β values for both amine- and thiol terminated OPE's found in the group of Wang are lower, 0.20 Å^{-1} (STM) [14] and 0.21 Å^{-1} (C-AFM) [15] respectively. In reference [16], a value of 0.32 Å^{-1} is found for a series of shorter molecules (benzene dithiol, OPE2DT and OPE3DT) in a STM break-junction experiment. The group of Wandlowski found a similar value of 0.33 Å^{-1} with the same batch of molecules as ours in a STM break-junction experiment. The same batch of molecules is also used in large area molecular junctions and yields a much lower β value of 0.15 Å^{-1} ascribed to the different coupling to one of the electrodes due to an interface layer (PEDOT:PSS) [6]. So our measurement technique reproduces quite well the values found in literature for β in OPEs. Moreover we can compare our results individually with the reported values in the literature. In figure 5.6 we plot the conductance values found for OPE2DT, OPE3DT and OPE4DT in our measurements and the ones found for the same molecules in the group of Wandlowski (university of Bern). In addition we show the conductance values of OPE3DT found in the literature. We notice here that all the values are consistent with each other and our results. Hence, our experimentally found conductance values and decay constant do confirm the validity of our measurement technique.

A logical next step is to investigate the conductance at finite biases in a similar way. For this we take the cross-section of the 2D histogram at various biases (250, 500, 750 and 1000 mV) in the same fashion as shown in figure 5.3. Already in figure 5.4 we notice that the dI/dV parabolic curves are steeper as the molecules get longer. In figure 5.7-A we plot the conductance values versus the molecular length to study the length dependence with increasing biases in more detail. The conductance values are taken from the 1D histograms extracted from the 2D histograms of figure 5.4, in figure 5.7-B we show the 1D histograms for OPE4DT for various bias voltages. First of all we notice a rough, but not exact, exponential dependence on length for all the biases. Note that for high biases (1V) the dependence on length of the conductance deviates from exponential. Hence, we can also extract a β value for the selected biases which is shown in figure 5.7-C. Surprisingly we find a clear trend in β, for increasing biases the β factor decreases in a non-monotonous way. How can we describe this behaviour of β?

Let us first go back to the analogy between molecular charge transport and

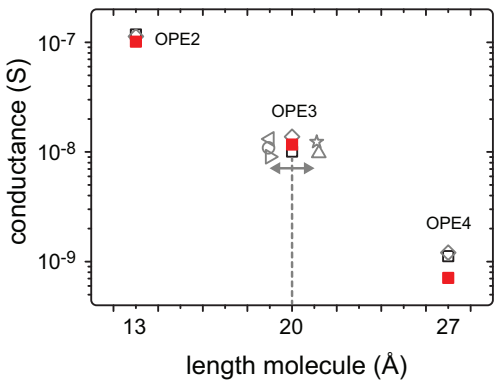

FIGURE 5.6: **Length dependence of the conductance compared to the literature values.** The filled squares are the zero bias conductances for our measurements. The open black squares are the values found by Wandlowski in liquid cell MCBJ. The gray open diamonds are from the same group but measured in a STM. For clarity we plotted the other literature values for OPE3DT with an artificial offset in the x direction (see arrows). (★) is from ref [17], (△) is from ref [18], (◁) is from ref [19], (▷) is from ref [20], (○) is from ref [16].

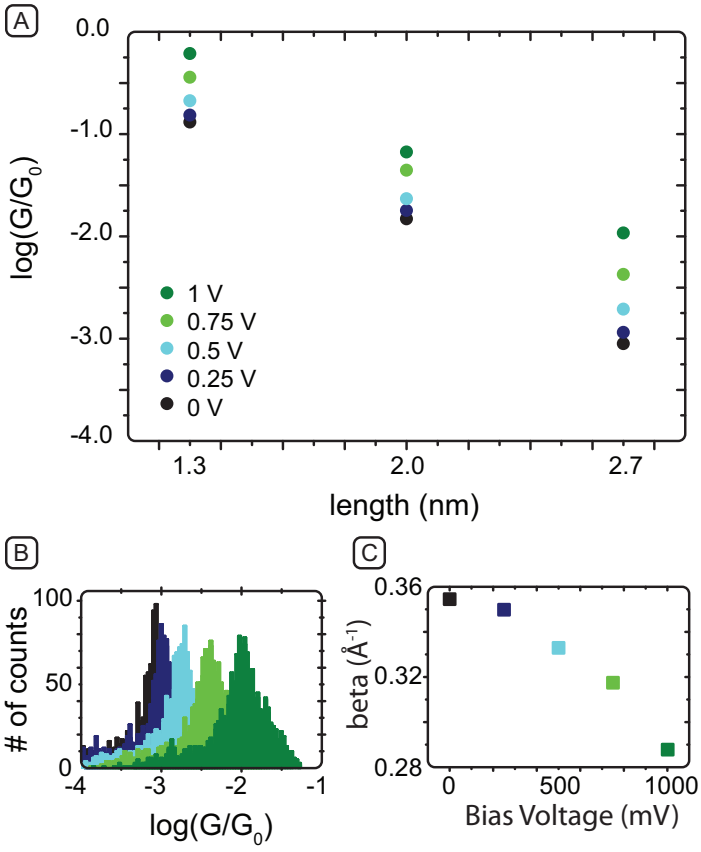

FIGURE 5.7: **Conductances for different bias voltages. A** Length dependence of the conduction for OPE2DT, OPE3DT and OPE4DT at different bias voltages. The conductance values are determined from the cross sections of the 2D histograms from figure 5.4 here shown for OPE4DT in **B C** Attenuation factor β for different bias voltages.

tunnel barriers in order to understand the obtained experimental results. The analogy made between molecular junctions and tunnel junctions rely on the experimental fact that the conductance is exponentially decreasing with increasing molecular length [1, 2, 21, 22]. We can describe a tunnel junction in a straight forward manner, shown in figure 5.8A and in equation 5.3. The resulting conductance G of a tunnel junction of width d, and height φ, the work function of the electrodes, can be expressed as follow:

$$G \propto \frac{2e^2}{h} \exp(-2\kappa d) \text{ where } \kappa = \sqrt{2m\varphi/\hbar} \tag{5.3}$$

Hence we see that the tunneling current is exponentially dependent on the distance and the square root of the work function of the electrodes. In a tunnel junction formed by STM or MCBJ one can continuously change the distance and measure the exponential current decay corresponding to this change [23]. Therefore measuring the current decay is a popular tool for the calibration of the distance in tunnel junctions e.g. STM or mechanically controlled break junctions (MCBJ) [24]. As we have seen in chapter 4, this is valid for low biases and not too small distances. Let us now have a critical look at the use and

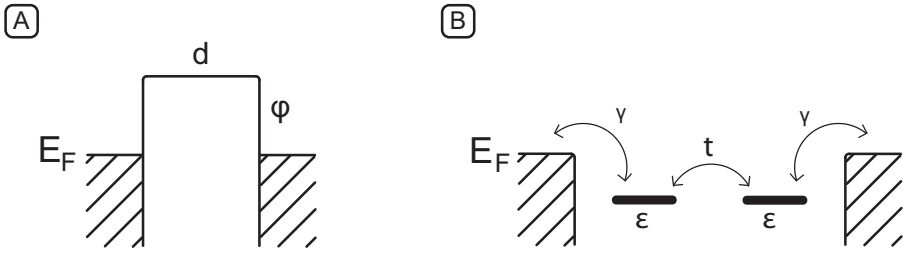

FIGURE 5.8: **Models for charge transport measurements. A** shows a rectangular tunnel barrier with heigth φ and length d. **B** shows a two site tight binding model with a hopping integral t between two site of energy ϵ and γ, the coupling to the leads. The leads are filled up to the Fermi energy E_F as indicated by the hatched lines.

meaning of the decay constant β for molecular charge transport. First we focus on the variation of the length. In contrast to tunnel junctions a molecular junction can not vary the inter-electrode distance continuously. Indeed the length of the different molecules used is changed by varying the number of sub-units e.g. pheny-ethynylene moieties in our case, so the inter-electrode distance is varying in discrete steps. Moreover in a tunnel junction, φ is defined by the work function of the electrodes and remains constant along the experiment. For a molecular junction this is less trivial. Indeed the height of the barrier is usually defined as the distance between the Fermi level and the closest molecular

orbital (HOMO or LUMO). As we will see later on, the position of the HOMO (or LUMO) is dependent on the molecular length, d for conjugated molecules. So in the tunnel barrier model, φ is dependent on d. The later makes it difficult to pin point a physical meaning to the experimentally measured exponential decay β as the barrier is changed for each measured molecule both in length and height. Moreover relating the measured β to a value for φ often results in unrealistic values or large discrepancies between experiment and fit [13, 25]. We should note here that the decay parameter β is poorly defined. However, our experimental findings can be understood in terms of molecular orbitals and resonant tunneling. Indeed a simple tight binding model (TB), introduced in chapter 1 and schematically depicted in figure 5.8-B, may provide a way to physically understand the length dependence of conductance in series of molecular junctions i.e. provide a more solid basis for the definition of β. Calculations of this type relate the rough chemical structure (number of repeating units) of a molecule to an energy dependent transmission function, T(E). Although more refined calculations take all the chemical structure factors into account[26–30], this simple model incorporates the basic physical concepts involved in molecular charge transport. The position of the HOMO (or LUMO) relative to the Fermi energy (E_F) is dependent on the number of hopping sites N and on the overlap integral t like described in equation 5.4 [26, 31].

$$E_{HOMO} = \varepsilon_0 - 2tcos(\frac{\pi}{N+1}) \tag{5.4}$$

Indeed by increasing the number N of sites i.e. the molecular length, we notice that the energy level closest to E_F moves towards E_F. In addition to that the coupling to the leads induces a broadening of the levels roughly exponentially decaying with length. This can easily be understood with simple arguments. The length dependence of the level broadening, $\Gamma(N)$ can be explained by the fact that the influence of the leads decays with increasing length, resulting in a smaller energy broadening. In addition, this broadening can be understood intuitively in terms of the uncertainty principle as the molecule gets longer, the residence time on it gets longer as well, resulting in a decrease of the broadening Γ [30].

Consequently we use this simple TB model to calculate a transmission function T(E) for toy molecules with increasing length i.e. the number of hopping sites. We can now investigate the implication of this more realistic model on the definition of β. In figure 5.9-A we present the calculated T(E) for molecules with a number of sites ranging from 1 to 5 sites. In this calculation the position of the Fermi level, E_F is arbitrary, in figure 5.9-A we show the Fermi level at three different positions. Note that the zero bias conductance is proportional to

the transmission function at the Fermi level. In figure 5.9-C we show the transmission values at the three positions of E_F (indicated in figure 5.9 by dashed lines) for the five toy molecules. First, we notice that when E_F is far away from the molecular levels (gray dashed line in figure 5.9-A) the transmission at the Fermi energy i.e. the zero bias conductance is exponentially dependent on the molecular length. Nevertheless for a Fermi energy closer to the levels we observe a deviation from the exponential behaviour. Moreover if the Fermi energy is found at or close to an energy where the transmission function cross, no or little length dependence will be observed[32].So the observation of an exponential length dependence of the conductance and the related β factor is strongly dependent on the position of the Fermi energy relative to the LUMO or HOMO.

In our experiment (figure 5.7 A and C) we observe a decrease in length dependence (β) for increasing bias voltage. So at higher voltages we integrate over a wider range, closer to the frontier molecular level, resulting in a shallower length dependence. Hence the toy model we use does reproduce qualitatively the trend observed in the experiments. In addition to that we have noticed in figure 5.9-D that for biases far from resonance the length dependence is exponential, while for bias windows reaching closer to the LUMO the length dependence deviates from exponential. This trend is of course more subtle to detect in our experiments due to the limited number of molecules (three different lengths) and the inherent spread of the conductance value as shown in the histograms. Still in figure 5.7-A we notice a slight deviation from exponential behaviour although more molecules are needed to make this point more solid. The range of biases we can apply, typically 1V, is not large enough to get closer to resonance and observe a clear deviation from exponential in the length dependence of conductance. Moreover the exponential length dependence of the conductance is observed when the Fermi level is far enough from the HOMO or LUMO. Oppositely, for a Fermi level closer to the HOMO or LUMO, the length dependence can be reduced or even disappear. More importantly this shows that the length dependence of the molecular conductance does not need to be exponential.

5.3.2 Looking at our measurements in the light of TVS

We discussed the limitations of transition voltage spectroscopy in chapter 4. To do so we first critically looked at TVS in the light of charge transport theory. This was followed by a comparison of measurements on vacuum tunnel barrier junctions and molecular junctions. Part of the results for the molecular junctions was taken from literature [33, 34] while the other part is taken from the

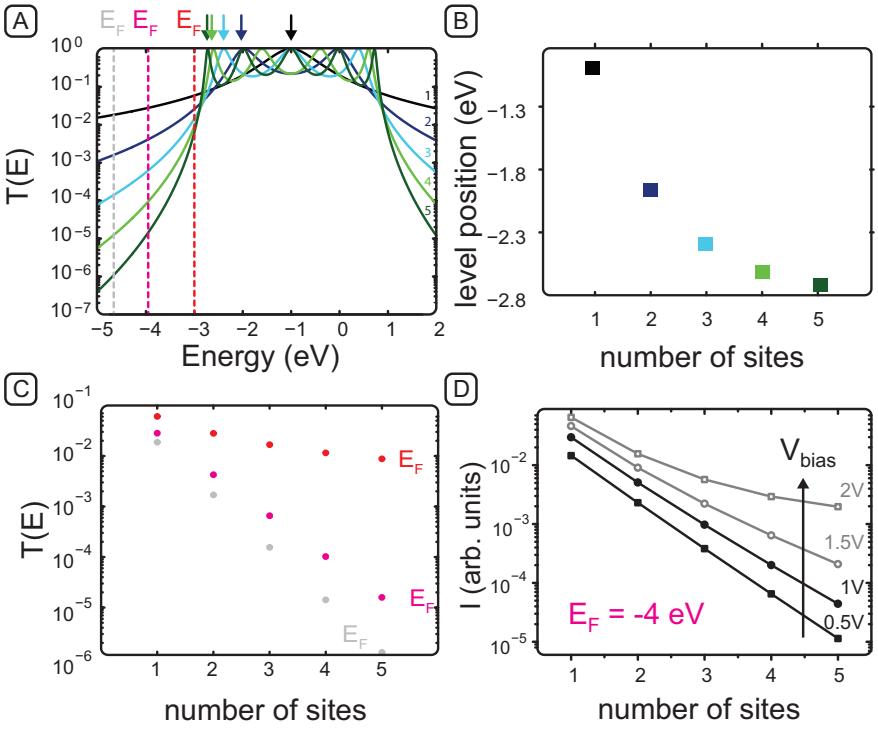

FIGURE 5.9: **Calculated T(E) at various energies for an increasing number of sites.** Calculations obtained with the simple toy model introduced in the main text. **A** Calculated energy dependent transmission functions for different molecular lengths. The parameters are: $t = 1$, $\varepsilon = -1$ and $\gamma_1 = \gamma_2 = 0.5$. **B** We show the position of the energy level closest to the Fermi energy as a function of the number of sites, the colours of the dots correspond to the colours of the transmission curves and the arrows indicating the levels in **A**. With the dashed lines we indicate three positions of the Fermi level. **C** Values of the transmission at the various Fermi energies as a function of the number of sites. The colours of the dots correspond to the colours of the dashed lines in **A**. **D** Calculated currents for different molecular length at increasing voltages.

measurements presented in this chapter on the OPEDT series. We describe here shortly the protocol used for the TVS results and the obtained results.

The basic idea of TVS is to plot the current-voltage characteristics on a Fowler-Nordheim plot i.e. $ln(I/V^2)$ vs $1/V$ which yields a minimum, V_m (see chapter 4). In figure 5.10-A we show one I(V) curve for OPE3DT and in figure 5.10-B the corresponding Fowler-Nordheim plot for positive bias voltages, we then clearly observe V_m.

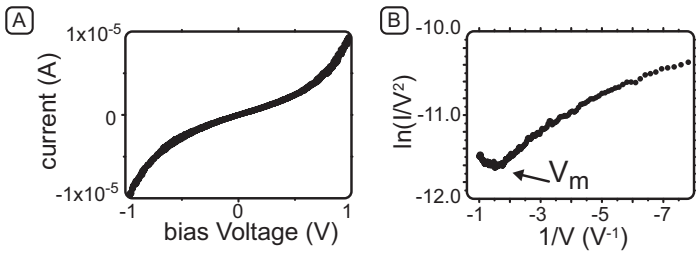

FIGURE 5.10: **How to make a Fowler-Nordheim plot. A** I(V) curve for OPE3DT. **B** corresponding Fowler-Nordheim plot for positive bias voltages.

For all the measurements presented above on OPE2DT, OPE3DT, OPE4DT and OPE3MT we computed the position of the minimum in the Fowler-Nordheim plot for both the negative bias, V_m^- and the positive bias, V_m^+. To represent the data in a statistical meaningful way, we choose to bin the V_m values and construct histograms for each molecule and bias polarity. In figure 5.11 we show the histograms for the four above mentioned molecules and show V_m^- and V_m^+ in two separate histograms.

The expectation of TVS is to relate the position of the closest level to the Fermi energy (HOMO or LUMO) with the position of V_m. Moreover we know from extended calculations[35] and optical measurements [35] that the HOMO is closer to E_F for longer molecules. So we expect to find a dependence of V_m with molecular length. However the nature of this relation is still unclear, as it has been showed by Mirjani et al. [31] and in chapter 4. More, experimentally challenging, ingredients are needed to extract information on the exact position of the molecular levels. Indeed we have seen in chapter 4 that knowledge on the junction's potential profile is essential for determining the position of molecular levels from V_m [31, 36]. In figure 5.11-A-C we do not observe the expected dependence of V_m on the length of the dithiolated molecules. Indeed for increasing molecular length it is not possible to distinguish any trends in the position of V_m. TVS is also limited by the intrinsic variation found in molecular junctions.

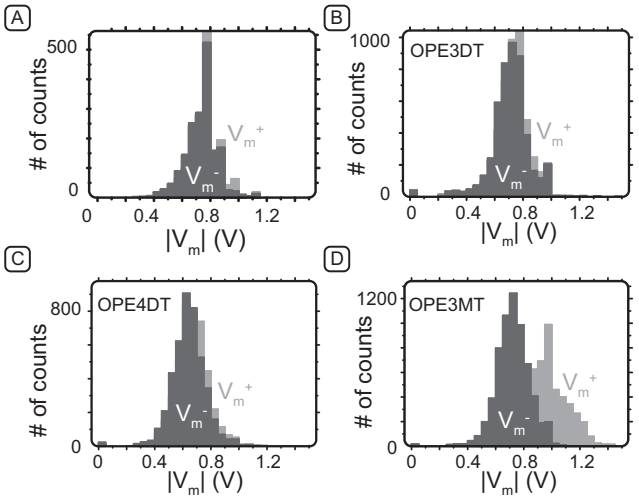

FIGURE 5.11: **Histograms for V_m^- and V_m^+ for OPE2DT A, OPE3DT B, OPE4DT C and OPE3MT D** Here the histograms for V_m^- and V_m^+ are presented. Note that we present here the absolute value of V_m.

Second we notice that for OPE2DT, OPE3DT and OPE4DT the values for V_m^- and V_m^+ are similar within the experimental error i.e. the histogram do fully overlap (figure 5.10-A-C). This is not true for OPE3MT as we can see on figure 5.10-D, indeed V_m^+ (0.92 V) is found at higher values than V_m^- (0.72 V). Let us discuss here the differences found between OPE3DT and OPE3MT. The dithiolated molecules (OPE2DT, OPE3DT and OPE4DT) have a sulfur atom at each extremities so that they can bind to both gold electrodes. In contrast monothiolated molecules, like OPE3MT, only posses one sulfur binding group to bind to the electrodes (in this case to the gold substrate when the SAM is formed). The junction symmetry determines the coupling, Γ, to the leads. The coupling Γ describes the extend to which the wave functions do overlap in a molecular junction. So for OPE3MT the overlap at one electrode is smaller than at the other one, reducing the total broadening (see chapter 1). Hence the conductances of the monothiolated species are lower than their dithiolated homologue (see figure 5.4). The symmetry in the binding groups do also influence the symmetry of the junction's potential profile, η (see chapter 1). So when $\eta = \frac{1}{2}$ the voltage drop is symmetric, while for $\eta = 0$ the voltage drop is completely asymmetric. Mirjani *et al.* demonstrated that we can relate η to V_m [31] as follow: $\frac{\eta}{1-\eta} = \frac{V_m^-}{V_m^+}$.

Hence, by comparing the histogram peaks found for V_m^+ and V_m^- in figure 5.11 for OPE2DT, OPE3DT, OPE4DT and OPE3MT we can calculate the parameter η for the four molecules: $\eta_{OPE2DT} = 0.49$, $\eta_{OPE3DT} = 0.5$, $\eta_{OPE4DT} = 0.5$ and $\eta_{OPE3MT} \approx 0.41$. The dithiolated molecules all have a $\eta \approx 1/2$ which is indeed expected for a symmetric junction. For OPE3MT, the junction is not completely asymmetric ($\eta = 0$) as still the molecule has some coupling to the electrodes at the side without thiol, resulting in a $\eta \neq 0$. Markussen *et al.* calculated for a similar junction a value for $\eta = 0.4$ which is quite in agreement with our experimentally found value for OPE3MT[37].

As a final remark, from the TVS on our measurements we can not determine the position of the molecular levels. nevertheless TVS can be useful for quantifying the (a)symmetry of molecular junctions.

5.4 Conclusions

To summarize, we present in this chapter C-AFM conductance measurements on a series of OPE molecules of various length. We introduced a new plotting method to present all the voltage dependent conductance data for each molecule at once in the form of a 2D histogram. Clearly, the measured zero-bias conductance values for OPE2DT, OPE3DT and OPE4DT are consistent with the literature, validating our C-AFM technique. Moreover we investigated the voltage dependence of the conductance and noticed a decrease in the "β" value for increasing biases. This voltage dependence of the conductance is consistent with simple calculations. Nonetheless we note that the length dependence of molecular conductance is not always exponential. Furthermore we probed the (a)symmetry of the molecular junctions (OPE3DT and OPE3MT) using TVS.

References

[1] B. Mann and H. Kuhn, *Tunneling through Fatty Acid Salt Monolayers*, Journal Of Applied Physics **42**, 4398 (1971).

[2] H. B. Akkerman and B. de Boer, *Electrical conduction through single molecules and self-assembled monolayers*, Journal Of Physics-Condensed Matter **20** (2008).

[3] H. B. Akkerman, P. W. M. Blom, D. M. de Leeuw, and B. de Boer, *Towards molecular electronics with large-area molecular junctions*, Nature **441**, 69 (2006).

[4] A. Salomon, D. Cahen, S. Lindsay, J. Tomfohr, V. B. Engelkes, and

C. D. Frisbie, *Comparison of electronic transport measurements on organic molecules*, Advanced Materials **15**, 1881 (2003).

[5] E. H. van Dijk, D. J. T. Myles, M. H. van der Veen, and J. C. Hummelen, *Synthesis and Properties of an Anthraquinone-Based Redox Switch for Molecular Electronics*, Organic Letters **8**, 2333 (2006).

[6] H. Valkenier, E. H. Huisman, P. A. van Hal, D. M. de Leeuw, R. C. Chiechi, and J. C. Hummelen, *Formation of High-Quality Self-Assembled Monolayers of Conjugated Dithiols on Gold: Base Matters*, Journal of the American Chemical Society **133**, 4930 (2011).

[7] X. Y. Xiao, B. Q. Xu, and N. J. Tao, *Measurement of single molecule conductance: Benzenedithiol and benzenedimethanethiol*, Nano Letters **4**, 267 (2004).

[8] X. Li, J. He, J. Hihath, B. Xu, S. M. Lindsay, and N. Tao, *Conductance of Single Alkanedithiols: Conduction Mechanism and Effect of Molecule-Electrode Contacts*, Journal of the American Chemical Society **128**, 2135 (2006).

[9] W. Haiss, R. J. Nichols, H. van Zalinge, S. J. Higgins, D. Bethell, and D. J. Schiffrin, *Measurement of single molecule conductivity using the spontaneous formation of molecular wires*, Physical Chemistry Chemical Physics **6**, 4330 (2004).

[10] M. T. Gonzalez, S. M. Wu, R. Huber, S. J. van der Molen, C. Schonenberger, and M. Calame, *Electrical conductance of molecular junctions by a robust statistical analysis*, Nano Letters **6**, 2238 (2006).

[11] V. B. Engelkes, J. M. Beebe, and C. D. Frisbie, *Analysis of the causes of variance in resistance measurements on metal-molecule-metal junctions formed by conducting-probe atomic force microscopy*, Journal Of Physical Chemistry B **109**, 16801 (2005).

[12] D. Fracasso, H. Valkenier, J. C. Hummelen, G. C. Solomon, and R. C. Chiechi, *Evidence for Quantum Interference in SAMs of Arylethynylene Thiolates in Tunneling Junctions with Eutectic GaIn (EGaIn) Top-Contacts*, Journal of the American Chemical Society **133**, 9556 (2011).

[13] H. B. Akkerman, R. C. G. Naber, B. Jongbloed, P. A. van Hal, P. W. M. Blom, D. M. de Leeuw, and B. de Boer, *Electron tunneling through alkanedithiol self-assembled monolayers in large-area molecular junctions*, Proceedings

Of The National Academy Of Sciences Of The United States Of America **104**, 11161 (2007).

[14] Q. Lu, K. Liu, H. Zhang, Z. Du, X. Wang, and F. Wang, *From Tunneling to Hopping: A Comprehensive Investigation of Charge Transport Mechanism in Molecular Junctions Based on Oligo(p-phenylene ethynylene)s*, ACS Nano **3**, 3861 (2009).

[15] K. Liu, G. R. Li, X. H. Wang, and F. S. Wang, *Length dependence of electron conduction for oligo(1,4-phenylene ethynylene)s: A conductive probe-atomic force microscopy investigation*, Journal of Physical Chemistry C **112**, 4342 (2008).

[16] Y. Xing, T.-H. Park, R. Venkatramani, S. Keinan, D. N. Beratan, M. J. Therien, and E. Borguet, *Optimizing Single-Molecule Conductivity of Conjugated Organic Oligomers with Carbodithioate Linkers*, Journal of the American Chemical Society **132**, 7946 (2010).

[17] J. Liao, M. A. Mangold, S. Grunder, M. Mayor, C. Schönenberger, and M. Calame, *Interlinking Au nanoparticles in 2D arrays via conjugated dithiolated molecules*, New Journal of Physics **10**, 065019 (2008).

[18] S. M. Wu, M. T. Gonzalez, R. Huber, S. Grunder, M. Mayor, C. Schonenberger, and M. Calame, *Molecular junctions based on aromatic coupling*, Nature Nanotechnology **3**, 569 (2008).

[19] X. Y. Xiao, L. A. Nagahara, A. M. Rawlett, and N. J. Tao, *Electrochemical gate-controlled conductance of single oligo(phenylene ethynylene)s*, Journal Of The American Chemical Society **127**, 9235 (2005).

[20] R. Huber, M. T. González, S. Wu, M. Langer, S. Grunder, V. Horhoiu, M. Mayor, M. R. Bryce, C. Wang, R. Jitchati, et al., *Electrical Conductance of Conjugated Oligomers at the Single Molecule Level*, Journal of the American Chemical Society **130**, 1080 (2008).

[21] C. D. Bain and G. M. Whitesides, *Attenuation Lengths of Photoelectrons in Hydrocarbon Films*, Journal of Physical Chemistry **93**, 1670 (1989).

[22] W. Wang, T. Lee, and M. A. Reed, *Mechanism of electron conduction in self-assembled alkanethiol monolayer devices*, Physical Review B **68**, 035416 (2003).

[23] G. Binnig, H. Rohrer, C. Gerber, and E. Weibel, *Surface Studies by Scanning Tunneling Microscopy*, Physical Review Letters **49**, 57 (1982).

[24] M. L. Trouwborst, C. A. Martin, R. H. M. Smit, C. M. Guedon, T. A. Baart, S. J. van der Molen, and J. M. van Ruitenbeek, *Transition Voltage Spectroscopy and the Nature of Vacuum Tunneling*, Nano Letters **11**, 614 (2011).

[25] W. Haiss, S. Martin, L. E. Scullion, L. Bouffier, S. J. Higgins, and R. J. Nichols, *Anomalous length and voltage dependence of single molecule conductance*, Physical Chemistry Chemical Physics **11**, 10831 (2009).

[26] F. Mirjani and J. M. Thijssen, *Density functional theory based many-body analysis of electron transport through molecules*, Physical Review B **83**, 035415 (2011).

[27] T. Markussen, R. Stadler, and K. S. Thygesen, *The Relation between Structure and Quantum Interference in Single Molecule Junctions*, Nano Letters **10**, 4260 (2010).

[28] M. P. Samanta, W. Tian, S. Datta, J. I. Henderson, and C. P. Kubiak, *Electronic conduction through organic molecules*, Physical Review B **53**, R7626 (1996).

[29] C. Joachim and M. A. Ratner, *Molecular electronics: Some views on transport junctions and beyond*, Proceedings Of The National Academy Of Sciences Of The United States Of America **102**, 8801 (2005).

[30] S. Datta, *Electrical resistance: an atomistic view*, nanotechnology **15**, S433 (2004).

[31] F. Mirjani, J. M. Thijssen, and S. J. van der Molen, *Advantages and limitations of transition voltage spectroscopy: A theoretical analysis*, Physical Review B **84**, 115402 (2011).

[32] G. Sedghi, V. M. Garcia-Suarez, L. J. Esdaile, H. L. Anderson, C. J. Lambert, S. Martin, D. Bethell, S. J. Higgins, M. Elliott, N. Bennett, et al., *Long-range electron tunnelling in oligo-porphyrin molecular wires*, Nature Nanotechnology **6**, 517 (2011).

[33] J. M. Beebe, B. Kim, C. D. Frisbie, and J. G. Kushmerick, *Measuring relative barrier heights in molecular electronic junctions with transition voltage spectroscopy*, Acs Nano **2**, 827 (2008).

[34] J. M. Beebe, B. Kim, J. W. Gadzuk, C. D. Frisbie, and J. G. Kushmerick, *Transition from direct tunneling to field emission in metal-molecule-metal junctions*, Physical Review Letters **97** (2006).

[35] H. Valkenier, Ph.D. thesis, Groningen University (2011).

[36] J. Z. Chen, T. Markussen, and K. S. Thygesen, *Quantifying transition voltage spectroscopy of molecular junctions: Ab initio calculations*, Physical Review B **82**, 121412 (2010).

[37] T. Markussen, J. Chen, and K. S. Thygesen, *Improving transition voltage spectroscopy of molecular junctions*, Physical Review B **83**, 155407 (2011).